A Simulation of Variability of ENSO Forecast Skill

M. K. DAVEY

Hadley Centre, U.K. Meteorological Office, Bracknell, United Kingdom

D. L. T. ANDERSON

Department of Physics, Clarendon Laboratory, Oxford, United Kingdom

S. LAWRENCE

Department of Physics and Astronomy, University of Leicester, Leicester, United Kingdom

(Manuscript received 27 May 1994, in final form 6 March 1995)

ABSTRACT

In many prediction schemes, the skill of long-range forecasts of ENSO events depends on the time of year. Such variability could be directly due to seasonal changes in the basic ocean–atmosphere system or due to the state of ENSO itself.

A highly idealized delayed oscillator model with seasonally varying internal parameters is used here to simulate such behavior. The skill of the artificial forecasts shows dependence on both seasonal and ENSO phase. Experiments with ENSO phase-locked to the seasonal cycle, but with no seasonal variation of model parameters, show that the ENSO cycle alone can induce variability in skill. Inclusion of seasonal parameters enhances seasonal skill dependence. It is suggested that the seasonal skill variations found in practice are due to a combination of seasonal changes in the basic state and the phase-locking of the ENSO and annual cycles.

1. Introduction

For the past few years dynamical forecasts of the El Niño–Southern Oscillation (ENSO) cycle in the tropical Pacific region have been made routinely using a coupled ocean–atmosphere model (Cane et al. 1986). The prediction skill is seasonally variable, with a marked decrease of skill commonly occurring in Northern Hemisphere spring. Similar seasonal skill variations occur in other dynamical and statistical ENSO forecast schemes, as discussed in the review by Latif et al. (1994). Skill may also vary with ENSO phase: Penland and Magorian (1993) find that their statistical forecasts are better for transitions between ENSO extremes than for peaks.

One possible cause of this variation in skill is that seasonal changes in the ocean–atmosphere system lead to different error growth conditions (Goswami and Shukla 1991; Blumenthal 1991; Webster and Yang 1992; Xue et al. 1994). Another reason may be that skill depends on the phase of ENSO: then any phase-locking of ENSO to the seasonal cycle will lead to seasonal skill dependence. Balmaseda et al. (1995) found strong seasonal skill dependence in the 1970s when ENSO was strongly phase-locked, but low seasonal skill dependence in the 1980s when ENSO was less phase-locked. The variation can depend on the skill measure being used: Xue et al. (1994) point out that low ENSO variance in northern spring is associated with low correlation skill, even though mean square forecast errors may not be larger than usual at that time.

In this note we use a highly idealized delayed-oscillator model to explore these mechanisms. The simple delayed oscillator is an ordinary differential equation for sea surface temperature anomalies in a region of strong ocean–atmosphere interaction, with the delay term accounting for the remote-forcing effect of equatorially trapped ocean waves that travel away from the interaction region and then return via reflection from coasts. Various forms of the delayed-oscillator equation have been used to help explain the oscillatory nature of ENSO (Schopf and Suarez 1988; Battisti and Hirst 1989; see the review by McCreary and Anderson 1991). The novel aspect here is that the parameters in such a model are allowed to vary seasonally, as described in section 2.

The behavior for several parameter choices is considered. In each case a control integration is made, followed by a series of "forecasts." Each forecast is initialized using control values plus random perturbations, then integrated forward for a few seasons. Standard

Corresponding author address: Dr. Michael K. Davey, Hadley Centre for Climate Prediction and Research, Meteorological Office, London Road, Bracknell, Berkshire RG12 2SY, United Kingdom.

forecast skill assessments are made: typical results are described in section 4. The model forecast skill usually varies markedly through the ENSO cycle. That cycle can be phase-locked to an integer number of years by either allowing the internal parameters to vary with season or by adjusting a timescale. We find that seasonal skill variations depend on both the phase-locking of ENSO and on internal parameter seasonality.

2. The delayed oscillator model

Battisti and Hirst (1989, BH89 hereafter) derived a hierarchy of simple linear and nonlinear equations as analogs to a more complex dynamical model based on that of Zebiak and Cane (1987). The equations determine the sea surface temperature anomaly T in a central-east region of the equatorial Pacific, where ocean–atmosphere interaction is concentrated. Locally there is a positive feedback mechanism operating: for example, a warm T anomaly will induce wind anomalies that decrease upwelling, which in turn increases T. The shape of the background ocean vertical temperature profile affects the influence of the upwelling. In particular, nonlinearity of the profile limits the amplitude of T anomalies. The wind anomalies also drive long equatorial Rossby waves that reflect from the western boundary to return to the interaction region as equatorial Kelvin waves. These waves affect the upwelling, and hence T, as a delayed feedback. This sustained feedback effect can reverse the local T anomaly and thus induce interannual oscillations that represent ENSO.

In BH89 the background vertical temperature profile has a tanh-like shape. For small disturbances this is represented by cubic nonlinearity in a delayed oscillator equation; for example, BH89 (4.6) is, in their notation,

$$T_t = cT - bT(t-\tau) - e[T - rT(t-\tau)]^3. \quad (1)$$

Here r represents the efficiency of wave reflection, and τ is the time for waves to travel from the interaction region to the boundary and back. The parameters c (positive feedback) and e (nonlinear amplitude limitation) are local to the interaction region. According to the BH89 definition, b is proportional to the reflection efficiency r, while b/r is local to the interaction region.

When disturbances are not small, it is better to retain the tanh dependence in some form for the nonlinear effects. We will use

$$T_t = cT + (b/r) \times ((1/A)\tanh[A(T - rT(t-\tau))] - T), \quad (2)$$

where $A^2 = 6er/b$. This form retains the simplicity of symmetry for warm and cold anomalies and reduces to (1) when the tanh term is approximated by linear and cubic terms for small amplitude. [Münnich et al. (1991) also use tanh dependence in a more complex model that allows asymmetry and includes several reflected waves from eastern and western boundaries.]

We define nondimensional variables $\hat{t} = c_0 t$, $\hat{T} = A_0 T$, to obtain

$$\hat{T}_{\hat{t}} = \gamma\hat{T} + (\alpha/r) \times \left(\frac{A_0}{A}\tanh\left[\frac{A}{A_0}(\hat{T} - r\hat{T}(\hat{t}-\Delta))\right] - \hat{T}\right), \quad (3)$$

where

$$\gamma = c/c_0, \quad \Delta = c_0\tau, \quad \alpha = b/c_0.$$

Here c_0 and A_0 are typical mean values for c and A. The factors A/A_0 enter the nonlinear effects: for simplicity, we shall omit seasonal variations in A to reduce (3) to

$$\hat{T}_{\hat{t}} = \gamma\hat{T} + (\alpha/r)(\tanh[\hat{T} - r\hat{T}(\hat{t}-\Delta)] - \hat{T}). \quad (4)$$

BH89 discuss the seasonal variation of their parameters. In the interaction region, upwelling is relatively weak in March–April, while the atmospheric response to SST anomalies is relatively strong at that time. The net effect is that b and c vary by about 10% (see, e.g., BH89 Figs. 14, 15), with b weakest in March–April and c weakest in November–December. The parameters r and τ vary little with season. We represent seasonality in our idealized model by simple sinusoidal terms:

$$\gamma = \gamma_0 + \gamma_1 \sin(2\pi\hat{t}/c_0), \quad (5a)$$

$$\alpha = \alpha_0 + \alpha_1 \sin(2\pi\hat{t}/c_0), \quad (5b)$$

with $\gamma_0 = 1$. Note that $\hat{t} = c_0$ corresponds to one year. Thus γ_1 represents seasonal variations in the parameter c, while α_1 represents variations in b. We will use $\alpha_1 < 0$ in later examples to represent the spring weakness of b noted by BH89.

Seasonal dependence could also be introduced by specifying some external forcing term, as in Wu et al. (1993) and Tziperman et al. (1994). The latter discuss nonlinear resonances with the seasonal cycle and the chaotic behavior that can occur as the system switches between different resonances.

Equation (1) is more analytically tractable when the delay term is omitted in the cubic term (see BH89 for example). The corresponding nondimensional form is

$$\hat{T}_{\hat{t}} = \gamma\hat{T} - \alpha\hat{T}(\hat{t}-\Delta) - (\alpha/6r)\hat{T}^3. \quad (6)$$

This is equivalent to the form discussed in McCreary and Anderson (1991), with the same α, Δ notation. [In McCreary and Anderson there is no seasonality, and the coefficient of the cubic term is 1: this latter is simply a rescaling of $\hat{T}$, which does not affect the stability properties of (6) as determined by α and Δ.]

Various stability properties of (4) are summarized in the appendix, and in Fig. 1, for fixed parameter values. For small delay Δ the system is stable, but oscillating solutions are found when Δ increases beyond

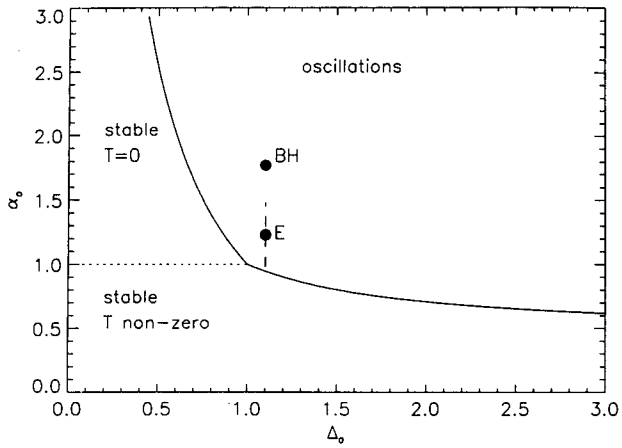

FIG. 1. Dependence of the stability of the delayed oscillator (4) on the parameters α_0 and Δ_0, for $\gamma = 1$. For $\alpha_0 < 1$ the critical curve is an estimate. Parameters for the cases BH and E described in the text are shown. The range of the seasonal cycle for α in case E2 is indicated by the dashed line.

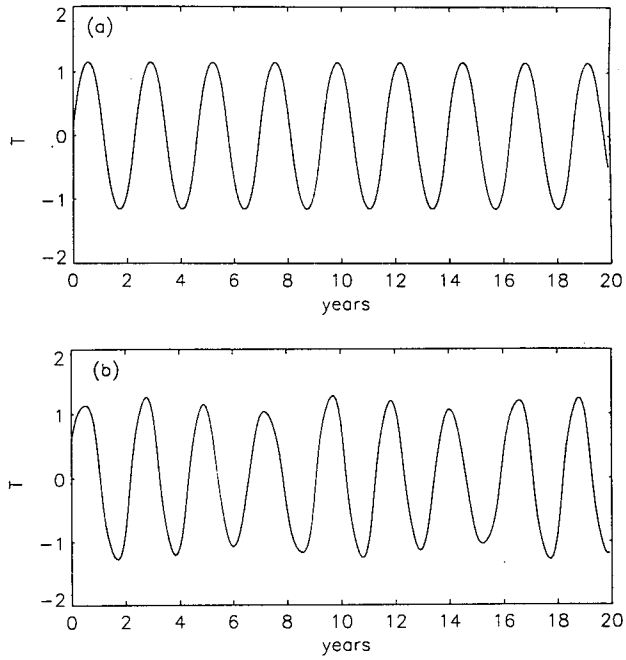

FIG. 2. Control values: (a) for case BH1 there is a regular oscillation; (b) for case BH2, with seasonal α, oscillations are irregular.

some critical value Δ_c. For $\alpha > \gamma$ the unique stable solution is $T = 0$ for small delay, whereas for $\alpha < \gamma$ there are multiple stable nonzero solutions for small delay.

The parameters chosen by BH89, based on their adaptation of the Zebiak and Cane model, are $r = 0.66$, $c_0 = 2.2\ \text{yr}^{-1}$, $b_0 = 3.9\ \text{yr}^{-1}$, $e = 0.07°\text{C}^{-2}\ \text{yr}^{-1}$, and $\tau = 0.5$ yr. The corresponding nondimensional values are $\alpha_0 = 1.77$, $\Delta = 1.1$. With these parameters and no seasonal dependence, (4) has the regular oscillatory solution shown in Fig. 2a, with a period of 2.3 years.

When α or γ was allowed to vary seasonally about the standard BH89 values, we found that the behavior became irregular (cf. Tziperman et al. 1994, with seasonal external forcing); an example is provided in Fig. 2b. In our experiments with (4), several other values of α_0 and Δ_0 were considered. For some of these cases parameter seasonality had the effect of phase-locking the interannual oscillations to a regular cycle with a period of an integer number of years: see, for example, case E2 in section 4. In another case the solution repeated every 12 years, with 5 irregular cycles within each 12 years. The behavior (irregular or phase-locked) evidently is sensitive to the choice of parameters. We have not explored the parameter space thoroughly enough to determine the parameter regimes for regular versus irregular behavior.

In some cases the seasonal range of α was extended across the stability boundary, so for a part of the seasonal cycle the system should be stable. This boundary crossing had no significant effect on the interannual oscillations for the cases considered: during brief excursions through stable regions of parameter space, the solution trajectories were maintained by the system memory induced by the delay term.

To illustrate variations in forecast skill in a simple way, we will mostly use a selection of the regular phase-locked cases that we found. The parameters for the particular cases discussed are summarized in Table 1 and Fig. 1. For brevity these cases only use seasonally varying α: however, similar general conclusions hold for seasonally varying γ.

3. Forecast method

Equation (4) was integrated using a time step δt set to the equivalent of 6 days (giving 60 steps per year, with a 360-day year for convenience). The temperatures T were saved after a spinup of several years. These temperatures provided control values C_i at monthly intervals, for N interannual cycles of K years each, giving a total of $12NK$ values. Forecasts F_{ij} were made of each C_i, with a lead time of j months. A forecast made from a time t_0 (say) was initialized by setting

TABLE 1. Parameters for selected cases. In each case $r = 0.66$, $\gamma_0 = 1$, $\gamma_1 = 0$. Parameters b_0 and c_0 have units per year, τ is in years.

Case	α_0	α_1	Δ_0	Period (yr)	b_0	c_0	τ
BH1	1.77	0	1.1	2.33	3.9	2.2	0.5
BH2	1.77	−0.35	1.1	irregular 2–3	3.9	2.2	0.5
BH3	1.77	0	1.1	3.00	3.0	1.71	0.64
BH4	1.77	−0.35	1.1	3.00	3.0	1.71	0.64
E1	1.23	0	1.1	3.87	2.7	2.2	0.5
E2	1.23	−0.25	1.1	4.00	2.7	2.2	0.5
E3	1.23	0	1.1	4.00	2.61	2.13	0.52

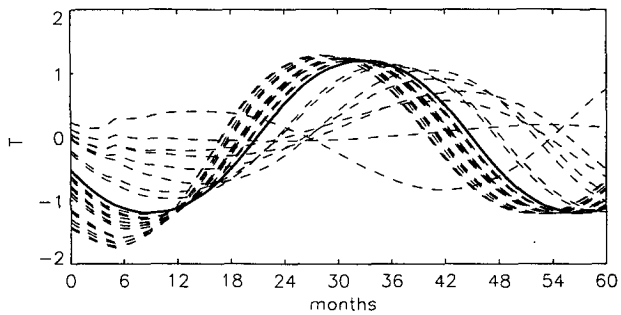

FIG. 3. Typical forecast trajectories (dashed) and the control (solid) taken from case E3. Each forecast shown starts from month 1 with different initial random perturbations from the control.

T to the saved control values in the "memory" period $t_0 - \Delta$ to t_0 and then adding random perturbations to those values. In some experiments only the last three values at t_0, $t_0 - \delta t$, and $t_0 - 2\delta t$ were perturbed. In other experiments the random perturbations were spread sparsely over the whole "memory," with linear interpolation between perturbed points, to provide lower frequency disturbances. In most cases described below, the control oscillates regularly with an interannual ENSO cycle of K years. Then, with each control ENSO cycle identical, the above process is equivalent to using N sets of initial perturbations for forecasts for one ENSO cycle. Typically $N = 50$ was large enough for statistical quantities to stabilize.

Figure 3 shows the evolution of some sample forecasts, from case E3, with each forecast starting at the same ENSO phase with the same memory but with different random initial perturbations. The memory component means that most forecasts tend to follow the same general trajectory. In this case each forecast will eventually settle itself into a regular oscillation, but not necessarily with the same phase as the control cycle. Note that for perturbations that generate unusually large values of T, the forecasts settle rapidly back toward the control cycle. By contrast, some forecasts that start with small T take several years to recover oscillatory behavior.

The forecasts were analyzed by taking averages with the interannual (for regular ENSO cycles of K years) or seasonal phase fixed. It is convenient to label values by writing

$$i = 12[(n-1)K + k - 1] + m = 12K(n-1) + l,$$

for month m of year k of cycle n ($m = 1 \cdots 12$, $k = 1 \cdots K$, $n = 1 \cdots N$), where $l = 12(k-1) + m$ for $l = 1 \cdots 12K$. Thus m is a label for the month of the year, and l is a label for the month (phase) of the interannual cycle. Note that a quantity labeled mj refers to forecasts *for* month of the year m, *starting* in month of the year $m_0 = (m - j)$ mod 12.

For example, with this notation the forecast mean for month of ENSO l and lead j is

$$\bar{F}_{lj} = \frac{1}{N}\sum_{n=1}^{N} F_{ij}.$$

The control mean $\bar{C}_l$ is similarly defined, and the systematic error is $S_{lj} = \bar{F}_{lj} - \bar{C}_l$. (Note that in the cases for which each control ENSO cycle is identical, $\bar{C}_l = C_l$.) The root-mean-square forecast errors e_{lj} for month of ENSO, and e_{mj} for month of year, are defined by

$$e_{lj}^2 = \frac{1}{N}\sum_{n=1}^{N}(F_{ij} - C_i)^2, \quad e_{mj}^2 = \frac{1}{K}\sum_{k=1}^{K} e_{lj}^2.$$

The forecast month of ENSO and month of the year standard deviations are denoted σ_{lj} and σ_{mj}, respectively. Control standard deviations are likewise denoted σ_l and σ_m. The month of the year correlation of forecasts and control is denoted r_{mj}.

4. Simulated forecast skill

Details of the parameters for all the cases discussed in this section are provided in Table 1.

a. *Case BH*

With constant parameters as in BH89 (case BH1), the system contains no seasonal information. There are regular oscillations (Fig. 2a), but ENSO peaks can occur at any time of year, and forecast skill is independent of month of the year m.

When α varies seasonally (case BH2), the interannual behavior is irregular (Fig. 2b), and for a large sample the control month of the year mean is near zero for all m. However, the control standard deviation σ_m and the forecast skill depend on m, albeit weakly. Figure 4 shows σ_m and e_{mj} at lead $j = 9$ months: the control variance is largest in April–May–June (as is the scatter in forecast values, not shown), and forecast rms error tends to be somewhat larger in February–March–April. Although the seasonal signal is weak, case BH2 demonstrates that seasonal parameter dependence can induce seasonal forecast dependence in our simple

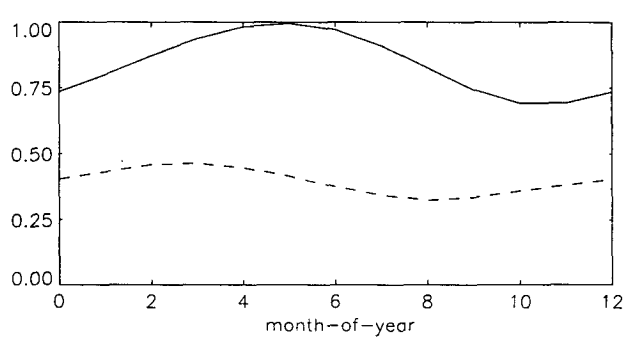

FIG. 4. Month of the year statistics for case BH2: control standard deviation σ_m (solid) and forecast rms error e_{mj} at lead $j = 9$ months (dashed).

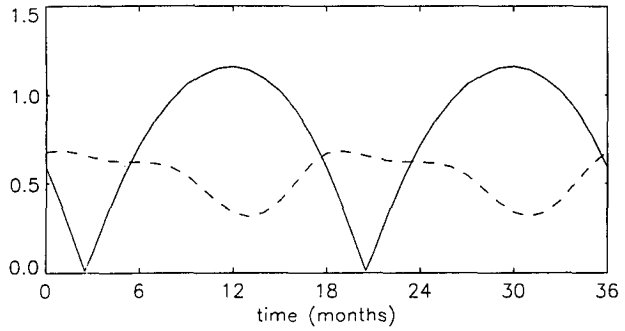

FIG. 5. Month of ENSO statistics for case BH3: control mean amplitude $|\bar{C}_l|$ (solid) and forecast rms error e_{lj} at lead $j = 9$ months (dashed).

model: this may be due to the direct effect of α on forecast error growth and/or due to the indirect effect of α in making ENSO depend on m in some way.

To isolate the latter effect, for case BH3 the timescale c_0^{-1} was adjusted to fix the ENSO cycle at exactly 3 years, while keeping α, Δ, and r constant with the same values as BH1. Figure 5 shows e_{lj} and $|\bar{C}_l|$ for $j = 9$ months. Forecast rms error is small when $|C|$ is large and relatively large when C is near zero (i.e., during transition from one extremum to another). A similar pattern is found for other lead times: errors are generally larger when forecasting for a transition and smaller when forecasting for a peak. This behavior is also typical of other cases examined. A plausible explanation for the reduced errors near extrema is that forecast amplitudes greater than the natural ENSO scale are suppressed by nonlinear effects. This suppression is reflected in reduced forecast scatter near ENSO extrema (low σ_{lj}) and in a systematic bias of forecasts to a mean amplitude smaller than the control near extrema.

Case BH3 thus shows that variations in ENSO amplitude alone can cause forecast skill to fluctuate through the ENSO cycle. Due to the ENSO period being an odd number of years for BH3, however, the extrema (and transitions) do not always occur at the same time of year. When month of the year statistics are calculated, the contributions from different ENSO phases lead to very low dependence of forecast skill on m. The control and forecast variances also have little dependence on m.

For case BH4, α varies seasonally as in BH2, but with the timescale tuned as in BH3. A regular ENSO oscillation with period of 3 years is again obtained, but in this case the seasonal parameter variations lock the ENSO phase to the seasonal cycle. Only two different control cycles are possible, in contrast to case BH3 for which any combination of ENSO and seasonal phase is possible. The variations in α also induce an asymmetry between successive ENSO extrema. If α is seasonally small (in March–April in our examples) as ENSO reaches a peak, then that peak is broadened. Conversely, peaks become narrower if α is relatively large at that time. In one possible control cycle a broad warm northern winter–spring El Niño peak alternates with a narrow cold summer La Niña roughly at 18-month intervals, while in the other cycle broad cold winter–spring La Niña alternates with narrow warm summer El Niño. Again, rms error e_{lj} is relatively small near cold and warm peaks (Fig. 6). There is no obvious seasonal signal in e_{lj}, and indeed the dependence of forecast skill on month of the year is found to be low. Although seasonal α phase-locks the ENSO peaks, it does not generate significant seasonal forecast skill dependence in this case.

b. Case E

We choose a nearby point in parameter space (case E, see Fig. 1 and Table 1) to explore the seasonal and ENSO phase effects further.

With no seasonal parameter variation (case E1), the system oscillates with period 3.87 years, and forecast skill is independent of month of the year m (cf. case BH1). When α is allowed to vary seasonally (case E2), the ENSO cycle phase-locks to regular oscillations with a 4-yr period, in contrast to the irregular behavior of case BH2 with seasonal α. The ENSO peaks are broadened compared to E1, with maximum amplitude occurring in March–April when α is seasonally relatively small (cf. the broadening effect in BH4). The peaks have relatively slow onset and fast decline. Figure 7 shows rms error e_{lj} for $j = 9$ and $|\bar{C}_l|$. (By $j = 9$ months the error is comparable to the control in this case. At shorter lead times e_{lj} is smaller, but the pattern is similar.) In this case seasonally varying α introduces a clear annual signal in e_{lj}. The behavior in Fig. 7 can be regarded as the superposition of two effects: as in previous examples, error tends to be low near ENSO extrema, and error tends to increase when α is seasonally small.

Since the ENSO period is an even number of years for E2, the peaks always occur in the same month of

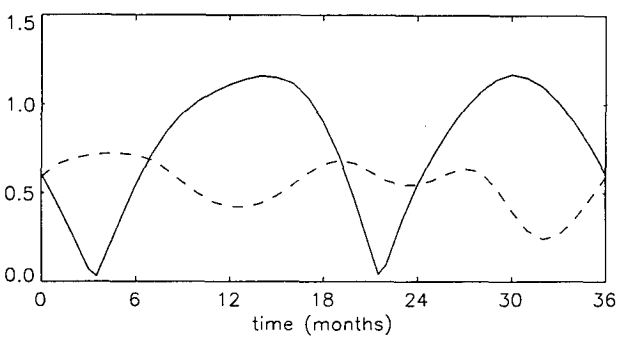

FIG. 6. Month of ENSO statistics for case BH4: control mean amplitude $|\bar{C}_l|$ (solid) and forecast rms error e_{lj} at lead $j = 9$ months (dashed).

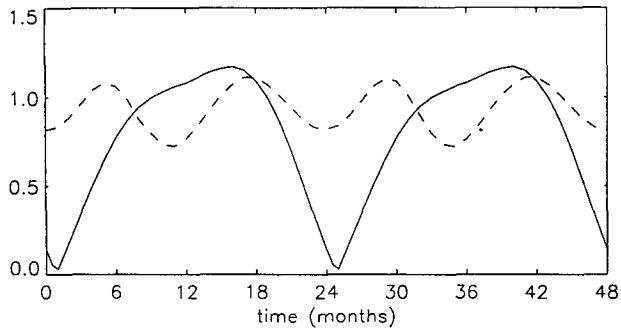

FIG. 7. Month of ENSO statistics for case E2: control mean amplitude $|\bar{C}_l|$ (solid) and forecast rms error e_{lj} at lead $j = 9$ months (dashed).

the year. The ENSO and seasonal phase effects on ENSO skill reinforce: consequently there is a clear dependence of forecast skill on month of the year m, in contrast to case BH3. Figure 8 shows the forecast versus control correlation r_{mj} as a function of lead time j and of month of the year m. For short lead times (up to 3 months) correlation skill is best for forecasts for May–June–July. Correlations decline as lead times increase: the most rapid decline is for forecasts starting in August–September–October, for which r is reduced to about 0.6 after 4 months. At lead times of 8–10 months, skill is lowest when forecasting April–May–June conditions. The behavior in this case shows that ENSO phase and seasonal basic-state effects can combine to create seasonal skill dependence. Examination of the rms error e_{mj} (not shown) leads to similar conclusions.

For case E3 we again attempt to isolate the ENSO phase-locking effect by adjusting the timescale to give an exact 4-yr cycle with constant parameters as in E1. A simple error pattern is found, with relatively low e_{lj} near ENSO peaks as usual, but no obvious annual signal in e_{lj}. With ENSO peaks always occurring at the same time of year, the month of the year statistics do show significant dependence on m, in contrast to BH3. The annual skill pattern is similar to that found for E2 but weaker in seasonal range.

5. Discussion

A simple delayed oscillator model has been used to simulate ENSO forecasts, with the aim of studying the possible effects of ENSO and seasonal phase on forecast skill. A tanh term was used to represent the nonlinearity inherent in upwelling effects that limits the growth of sea surface temperature anomalies T. The model includes parameters γ and α that can vary seasonally to represent the annual cycle of the basic state. Forecasts were made by using initial conditions created by randomly perturbing a control integration. Forecast versus control rms error and correlation were used as skill measures. Several features were found in a range of experiments. In the particular cases described, only the parameter α was allowed to vary seasonally.

The forecast error was generally smaller when target T anomalies were larger. That is, forecasts were more accurate when predicting El Niño and La Niña extrema than when predicting conditions during the transition from one extremum to another. The reduced error near extrema is likely to be partly due to nonlinear effects: any excessively large anomalies (i.e., values outside the normal range of interannual oscillation) produced by the forecasts were rapidly reduced by local feedbacks. Rms errors are also reduced near peaks simply because the control curve (the target of the forecasts) is flatter there.

The seasonal variation of parameters had several effects. The addition of seasonality could cause regular oscillations to become irregular in some cases (e.g., case BH2) and could induce phase-locking to a regular interannual cycle with a period of an integer number of years in other cases (e.g., E2). Parameter seasonality alone was sufficient to induce weak seasonal forecast skill variations, even if the model ENSO was irregular (BH2). Seasons when α was relatively small were generally associated with larger error. Seasonally smaller α was also associated with the broadening of an ENSO extremum if it occurred at that time of year: likewise, larger α tended to cause narrower extrema.

When ENSO was phase-locked to a period of an even number of years (i.e., such that peaks always occurred in the same month of the year), then the systematic reduction of forecast error near peaks led to a substantial seasonal signal in forecast skill. This is purely an ENSO phase effect: a seasonal skill signal was evident when ENSO was artificially phaselocked by altering the timescale, with no seasonal parameter dependence (E3). When ENSO was phaselocked by means of an annual parameter cycle, then the ENSO phase and the annual parameter phase effects on forecast skill combined to enhance the seasonal skill variations (E2). These seasonal skill variations were gradual, rather than sharp like the "spring barrier" some-

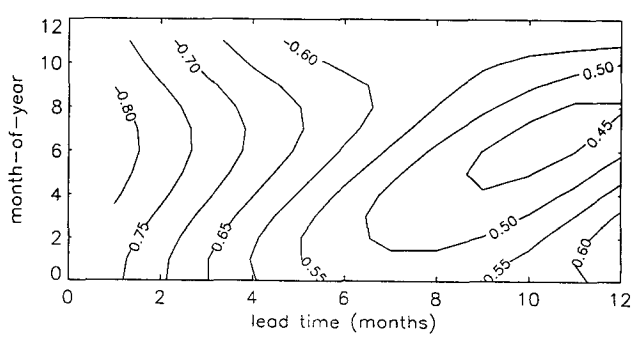

FIG. 8. Forecast versus control correlation r_{mj} for case E2 as a function of month of the year m and lead time j months.

times found in practice. This difference could be due to the smooth and limited parameter seasonality that we used or to the simplicity of our model.

These artificial ENSO forecasts suggest that seasonal variations in forecast skill can be due to the phase-locking of ENSO itself to the seasonal cycle, as well as to seasonal variations in the basic state of the system. Seasonality of ENSO predictions in practice has been found in several schemes. Further investigations to determine the extent of the ENSO phase effect are recommended.

The extent of seasonality in skill can depend on the measure used. Xue et al. (1994) pointed out the effect of variance on correlation skill. In our examples, rms error and correlation measures were considered. Other skill scores such as LEPS (Potts et al. 1995) may be less sensitive to the effects of seasonal and ENSO cycles and should be tested on ENSO predictions.

Acknowledgments. Anonymous referees provided useful comments: in particular a tanh form was recommended in place of the cubic nonlinearity used in the original version of this paper.

APPENDIX

Stability of the Delayed Oscillator Model

For fixed values of r, α, Δ, and γ, the following stability properties can be readily deduced for (4) (cf. Battisti and Hirst 1989; McCreary and Anderson 1991).

a. $\Delta = 0$ (no delay)

For $\alpha > \gamma$, the only stable solution is $\hat{T} = 0$.

For $r\gamma < \alpha < \gamma$, there are two stable nonzero equilibria of opposite sign, and $\hat{T} = 0$ is unstable.

For $\alpha < r\gamma$, there is unphysical unlimited growth.

b. $\Delta > 0$

As Δ is increased from zero to beyond some critical value Δ_c, the stable solutions above become unstable and the system oscillates.

For $\alpha > \gamma$ we can use a small amplitude expansion to find that $\hat{T} = 0$ becomes unstable for $\Delta > \Delta_c = \text{acos}(\gamma/\alpha)/(\alpha^2 - \gamma^2)^{1/2}$.

For $\alpha < \gamma$ the nonzero equilibria become unstable. The equilibria can be estimated as $\hat{T} = \pm(\gamma - \alpha)^{1/2}$, and an estimate for the stability boundary is $\Delta_c = \text{acos}(\beta/\alpha)/(\alpha^2 - \beta^2)^{1/2}$ with $\beta = 3\alpha - 2\gamma$. In some parts of parameter space both steady and oscillatory solutions can be found.

c. $r = 0$ (no reflection)

In this limit, interaction is purely local. Note that α is proportional to r, so α/r is independent of reflection.

For $\alpha/r > 1$, there are two nonzero stable equilibria and $\hat{T} = 0$ is unstable.

For $\alpha/r < 1$, behavior is unphysical (unbounded growth).

Note that stable equilibrium with $\hat{T} = 0$ is only attainable with reflection $r > 0$.

REFERENCES

Balmaseda, M. A., M. K. Davey, and D. L. T. Anderson, 1995: Decadal and seasonal dependence of ENSO prediction skill. *J. Climate,* **8,** 2705–2715.

Battisti, D. S., and A. C. Hirst, 1989: Interannual variability in a tropical atmosphere–ocean model: Influence of the basic state, ocean geometry, and nonlinearity. *J. Atmos. Sci.,* **46,** 1687–1712.

Blumenthal, M. B., 1991: Predictability of a coupled ocean–atmosphere model. *J. Climate,* **4,** 766–784.

Cane, M. A., S. E. Zebiak, and S. C. Dolan, 1986: Experimental forecasts of El Niño. *Nature,* **321,** 827–832.

Goswami, B. N., and J. Shukla, 1991: Predictability of a coupled ocean–atmosphere model. *J. Climate,* **4,** 3–22.

Latif, M., T. P. Barnett, M. A. Cane, M. Flügel, N. E. Graham, H. von Storch, J.-S. Xu, and S. E. Zebiak, 1994: A review of ENSO prediction studies. *Climate Dyn.,* **9,** 167–179.

McCreary, J. P., and D. L. T. Anderson, 1991: An overview of coupled ocean–atmosphere models of El Niño and the Southern Oscillation. *J. Geophys. Res.,* **96,** 3125–3150.

Münnich, M., M. A. Cane, and S. E. Zebiak, 1991: A study of self-excited oscillations of the tropical ocean–atmosphere system. *J. Atmos. Sci.,* **48,** 1238–1248.

Penland, C., and T. Magorian, 1993: Prediction of Niño 3 sea surface temperatures using linear inverse modeling. *J. Climate,* **6,** 1067–1076.

Potts, J. M., C. K. Folland, I. T. Jolliffe, and D. Sexton, 1996: Revised "LEPS" scores for assessing climate model simulations and long-range forecasts. *J. Climate,* **9,** 34–53.

Schopf, P. S., and M. J. Suarez, 1988: Vacillations in a coupled ocean–atmosphere model. *J. Atmos. Sci.,* **45,** 549–566.

Tziperman, E., L. Stone, M. A. Cane, and H. Jarosh, 1994: El Niño chaos: Overlapping of resonances between the seasonal cycle and the Pacific ocean–atmosphere oscillator. *Science,* **264,** 72–74.

Webster, P. J., and S. Yang, 1992: Monsoon and ENSO: Selectively interactive systems. *Quart. J. Roy. Meteor. Soc.,* **118,** 877–926.

Wu, D.-H., D. L. T. Anderson, and M. K. Davey, 1993: ENSO variability and external impacts. *J. Climate,* **6,** 1703–1717.

Xue, Y., M. A. Cane, S. E. Zebiak, and M. B. Blumenthal, 1994: On the prediction of ENSO: A study with a low-order Markov model. *Tellus,* **46A,** 512–528.

Zebiak, S. E., and M. A. Cane, 1987: A model El Niño–Southern Oscillation. *Mon. Wea. Rev.,* **115,** 2262–2278.